EasyChair Preprint

№ 3440

A Low-Cost Environmental Nitrate Sensor

Robert Dean, Elizabeth Guertal and Adam Newby

May 18, 2020

A Low-Cost Environmental Nitrate Sensor

Robert N. Dean
ECE Dept.
Auburn University
Auburn, AL USA
deanron@auburn.edu

Elizabeth A. Guertal
Crop, Soil & Eviro. Sci. Dept.
Auburn University
Auburn, AL USA
guertea@auburn.edu

Adam F. Newby
Horticulture Dept.
Auburn University
Auburn, AL USA
adam.f.newby@gmail.com

***Abstract*—Nitrates are nutrients important to commercial, residential, and agricultural applications. However, nitrate loss from these applications, and animal manures, is a major source of water pollution, leading to algae blooms and hypoxic dead zones in coastal waterways. Low-cost nitrate sensors would aid in preventing over application of nitrate based fertilizers and in monitoring the environment for nitrate based water pollution. Printed circuit board (PCB) technology is being used to realize a variety of low-cost environmental sensors. Here, a capacitive PCB sensor was swept in frequency, yielding a distinctive equivalent capacitance versus frequency signature with a characteristic resonant peak. Concentrations of three different nitrate solutions were evaluated with the sensor, producing resonant peaks that decrease in magnitude and frequency with increasing concentration. The data was used to define equations that map nitrate concentration to either resonant peak frequency or magnitude, with R^2 values greater than 0.95.**

Keywords—sensors, nitrates, pollution, precision agriculture

I. Introduction

Nitrates are salts that contain the NO_3^- anion. Examples include potassium nitrate (KNO_3), sodium nitrate ($NaNO_3$), and ammonium nitrate (NH_4NO_3). Nitrates are important nutrients for both animals and plants. Excessive levels of nitrates, however, have deleterious effects. In animals and humans, high levels and nitrates are toxic, and result in diseases such as methemoglobinemia [1]. Agricultural loss from excessive application of fertilizers to row crops such as corn and soybeans [2], as well as movement from livestock manure [3], are important sources of environmental nitrate pollution. In addition to agricultural sources, fertilizer loss from over application to urban lawns is also a major contributor to nitrate pollution in waterways [4]. Streams and rivers can transport these large concentrations of nitrates into coastal waterways, leading to eutrophication and the resulting algae blooms and hypoxic dead zones [5].

A low-cost sensor for detecting environmental nitrate levels would be beneficial for detecting nitrate pollution in waterways, for managing the disposal of livestock manure, and for optimizing agricultural, residential, and commercial fertilizer application. Although expensive commercial nitrate sensing systems exist, various techniques have been proposed for innovate nitrate sensors, including chemFETs [6], screen printed nitrate-selective electrodes [7], K ratio spectrophotometry [8], etched fiber Bragg gratings [9], and a Parylene-coated interdigital sensor [10]. Commercially available nitrate sensors often use ion-selective electrodes and cost a few hundred dollars (U.S. dollars) or more [11] [12]. In this work, a low-cost nitrate sensor is presented that consists of a frequency swept fringing field interdigitated electrode sensor realized using just low-cost commercial printed circuit board (PCB) technology.

II. Background

A. PCB Environmental Sensors

PCB technology has been used to realize a variety of low-cost miniaturized environmental sensors, for applications such as drought monitoring [13], measuring soil moisture content [14], and detecting water pollution [15]. In PCB based sensors, the standard materials and fabrication processes for manufacturing standard PCBs are used to realize electrodes for sensing functions. In some instances, additional materials and processes are added [14]. The basic materials include the circuit board substrate, the patterned Cu cladding, plated vias, patterned solder mask, and surface finishes applied to exposed Cu features. FR-4 E-glass is an electrical grade fiberglass with an organic resin binder and is useful as a rigid substrate for the sensor or sensing platform. Cu cladding can be used for electrical traces and for sensing electrodes. Solder mask is a polymeric material useful as a non-conductive moisture barrier layer over Cu electrodes. Surface finishes exist, such as plated Au, that can protect exposed electrodes from corrosive operating environments. Compared to other technologies such as MEMS, PCB sensors can have the advantages of low-cost development, quick fabrication times, and much larger sensing areas than can be implemented in traditional MEMS technologies.

B. Electrochemical Impedance Spectroscopy

When ionic compounds dissolve in water, they change the electrochemical properties of the resulting aqueous solution. In addition to increasing the electrical conductivity, they also form hydration shells that have relatively low resonant frequencies, on the order of tens of MHz [16]. If the aqueous solution is excited with electromagnetic energy at that frequency, the hydration shells will undergo dielectric relaxation as they are induced to vibrate at their natural frequency. These two effects measurably alter the impedance of the sensor and can be used to determine useful information about the chemistry of the aqueous solution. This was previously demonstrated with a PCB fringing field sensor tested in various aqueous solutions, which yielded plots of the sensor's equivalent parallel capacitance versus frequency [17]. A plot of that sensor's equivalent parallel capacitance versus frequency is presented in Fig. 1, where Tap was local tap water, 101010 was 10-10-10 fertilizer in tap water, Dist was distilled water, PO was water from the Pacific Ocean, Ammonia was ammonia in tap water,

Rain was local rain water, AmSu was ammonium sulfate in tap water, DI was deionized water, SS was hypersaline water from the Salton Sea, and Bleach was bleach in tap water. As the plot demonstrates, DI water resulted in the largest magnitude resonant peak at the highest frequency. Different aqueous solutions resulted in a shift in the resonant peak to a lower frequency and a smaller magnitude, depending on the electrochemical properties of the individual aqueous solution being evaluated with the PCB sensor. This process for evaluating chemical properties is called electrochemical impedance spectroscopy (EIS).

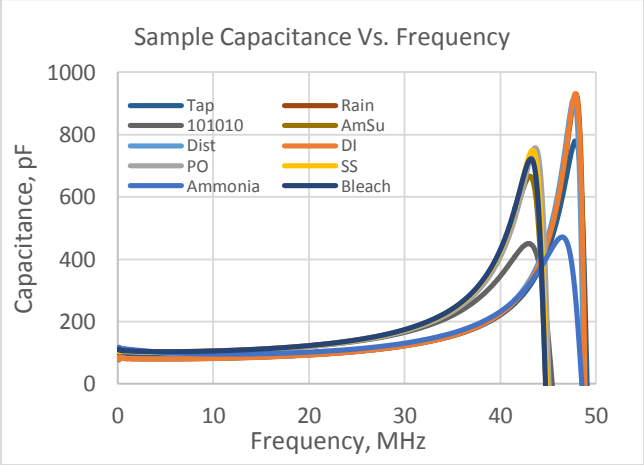

Fig. 1. A plot of the sensor's equivalent parallel capacitance versus frequency in various aqueous solutions [17].

III. Sensor Development

The EIS sensor developed for this application was implemented as an insulated fringing field sensor in a low-cost commercially available PCB fabrication process. A photograph of the sensor is shown in Fig. 2, where the sensor's active area is inside the white silkscreen rectangle on the left side of the photograph. The sensor consisted of an interdigitated electrode (IDE) array implemented in the patterned Cu cladding on the top side of a 2-layer FR-4 PCB, where 1 ounce Cu cladding was used. The interdigitated electrode array, a drawing of which is shown in Fig. 3, was insulated from the operating environment with an overcoat layer of polymeric solder mask. The circuit board for the sensor was 1.4 cm wide and 9.7 cm long. The 2.18 cm by 1.11 cm sensing electrode array consisted of 36 opposing electrode pairs. Each pair consisted of two 152.4 µm wide electrodes with a nominal overlap of 10.46 mm and a separation distance of 152.4 µm. 304.8 µm wide Cu signal traces ran under the solder mask layer from the electrode array to an attached SMA connector at the opposite end of the circuit board. The sensor board fabrication was outsourced to Osh Park using their low-cost 2-layer PCB prototyping service. In small quantities, the sensor PCB cost $3.52 (U.S. dollars). Electrically, the sensor was primarily a capacitor at low frequencies, where a sizable portion of the capacitance was due to the fringing fields that extended above the solder mask layer into the volume of space above the circuit board.

Fig. 2. A photograph of the fabricated PCB sensor.

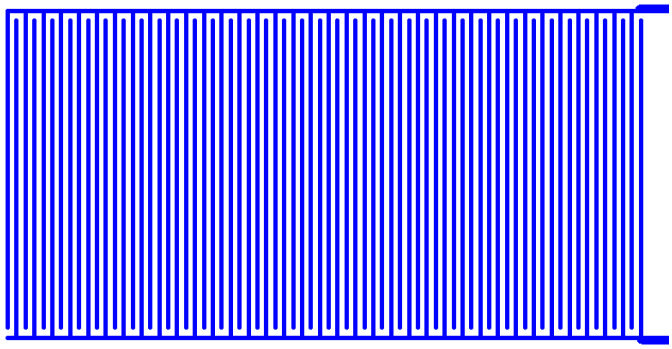

Fig. 3. A drawing of the PCB sensor's interdigitated electrode array structure.

The sensor was evaluated using an Agilent E35061B ENS series network analyzer via a coaxial cable. 125 mL Nalgene® containers were used for holding the various samples being evaluated, and the sensor PCB was designed so that it fit into the opening in the top of the container. A photograph of the test setup if presented in Fig. 4. The analyzer was configured for an S_{11} measurement and calculated the equivalent parallel capacitance as a function of frequency over the range of 100 KHz to 50 MHz, with a step size of 31.1875 KHz. 50 runs were taken and averaged to minimize the effects of uncorrelated noise in the measurements.

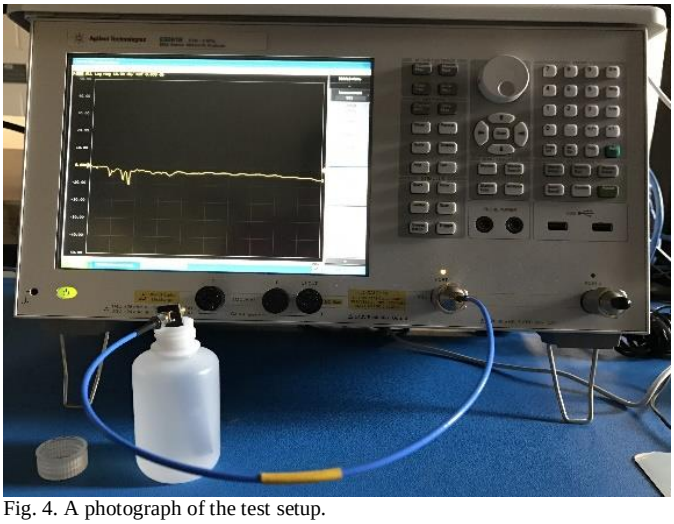

Fig. 4. A photograph of the test setup.

With the E35061B configured as described above, DI water was analyzed in ambient laboratory conditions (18°C and 44% RH). The resulting capacitance versus frequency data was plotted as shown in Fig. 5. At low frequencies, the reactance of the sensor in DI water is capacitive with a capacitance of approximately 100 pF. The plot has a distinctive resonant peak at approximately 42.64 MHz of 1136 pF. Above this frequency, the capacitance quickly decreases, and at approximately 43.54 MHz, the reactance becomes inductive. This plot represents a

distinctive electrochemical signature that can be used for comparison with other solution chemistries.

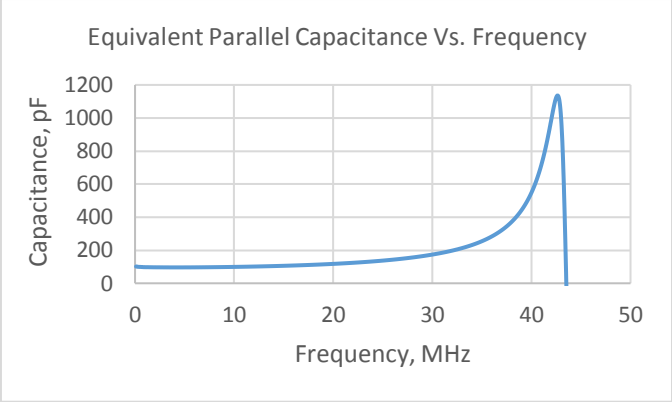

Fig. 5. A plot of equivalent parallel capacitance versus frequency for the PCB sensor in DI water.

IV. Nitrate Solution Testing

Although commercially available nitrate sensors often do not distinguish between different types of nitrate, three different nitrate solutions were investigated here: potassium nitrate (KNO_3), sodium nitrate ($NaNO_3$), and ammonium nitrate (NH_4NO_3). Aqueous solutions were made with DI water in concentrations of 10, 20, 40, 80 and 160 ppm with each of the three nitrates evaluated. The solutions were allowed to equilibrate to the air temperature in the laboratory, 18°C, prior to testing. Each solution was evaluated with the PCB sensor used to produce the parallel capacitance versus frequency plot in Fig. 5. In between individual tests, the sensor was rinsed in DI water. A series of parallel capacitance versus frequency plots for DI water and the various concentrations of KNO_3 are presented in Fig. 6. As the concentration of KNO3 increased, the magnitude and the frequency of the resonant peak decreased. The same characteristic was observed in the capacitance versus frequency plots for the $NaNO_3$ solutions (Fig. 7) and the NH_4NO_3 solutions (Fig. 8).

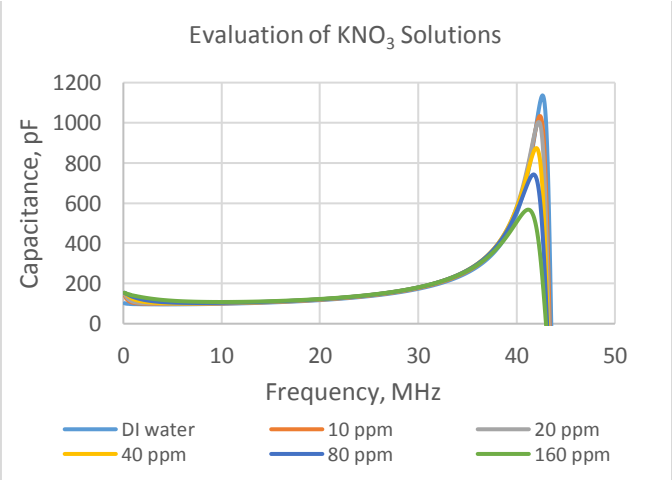

Fig. 6. A plot of the parallel capacitance versus frequency measurements for the KNO_3 solutions.

For each nitrate solution type and concentration, the magnitudes and frequencies of the corresponding resonant peaks are presented in Table I. The concentration of 0 ppm was the DI water test. For all the solutions evaluated, the magnitude and the frequency of the resonant peaks shifted to lower values as the concentration increased, with small differences observed between the three different nitrates evaluated.

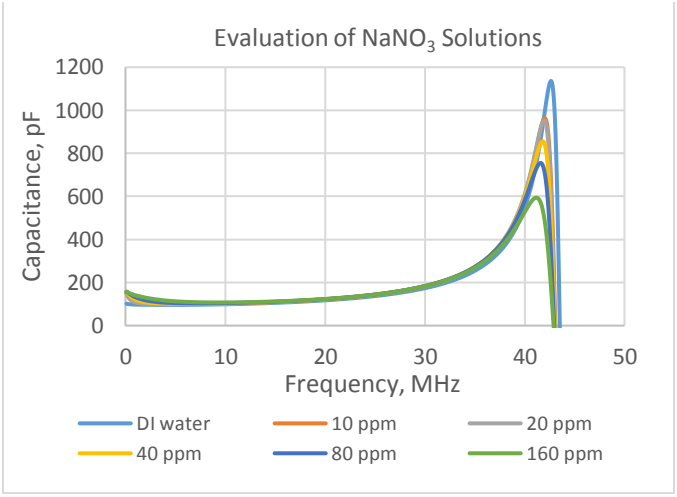

Fig. 7. A plot of the capacitance versus frequency measurements for the $NaNO_3$ solutions.

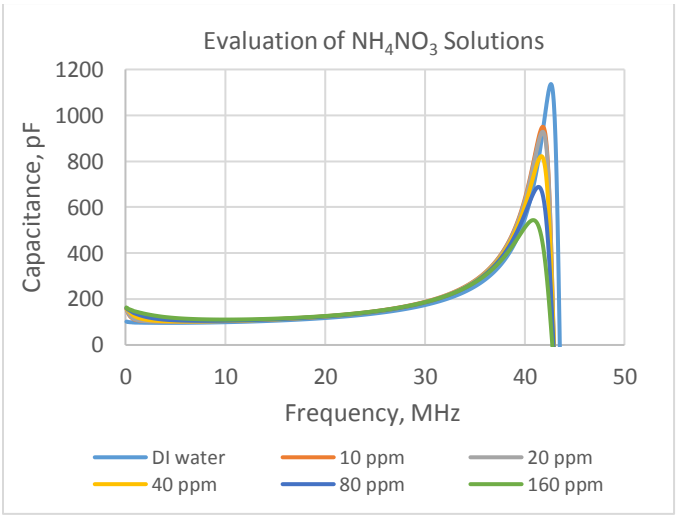

Fig. 8. A plot of the capacitance versus frequency measurements for the NH_4NO_3 solutions.

A plot of the frequency of each nitrate solution's resonant peak versus the solution's concentration is presented in Fig. 9. Similarly, a plot of the magnitude of each solution's resonant peak versus the solution's concentration is presented in Fig. 10. The traces in both plots reveal a nonlinear relationship between a nitrate solution's concentration and the location and magnitude of the solution's resonant peak when evaluated with the PCB sensor. In Figs. 8 and 9, second order polynomial trendlines were applied to the KNO_3, $NaNO_3$ and NH_4NO_3 data, respectively. R^2 values for fitting the data sets to these

trendlines are reasonably good, with values ranging from 0.8487 to 0.9932.

TABLE I. PEAK MAGNITUDE AND FREQUENCY DATA

	KNO_3		$NaNO_3$		NH_4NO_3	
Concen (ppm)	*Mag (pF)*	*Freq (MHz)*	*Mag (pF)*	*Freq (MHz)*	*Mag (pF)*	*Freq (MHz)*
0	1136.39	42.64	1136.39	42.64	1136.39	42.64
10	1034.01	42.39	962.91	42.02	949.95	41.83
20	1003.53	42.27	951.46	41.95	928.37	41.8
40	873.81	42.02	856	41.8	822.1	41.67
80	742.7	41.74	755.41	41.61	688.23	41.39
160	567.66	41.17	594.07	41.14	543.67	40.86

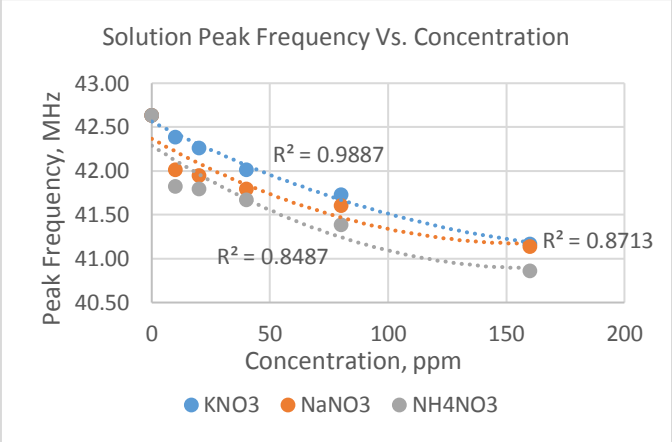

Fig. 9. A plot of solution peak frequency versus concentration for each nitrate evaluated.

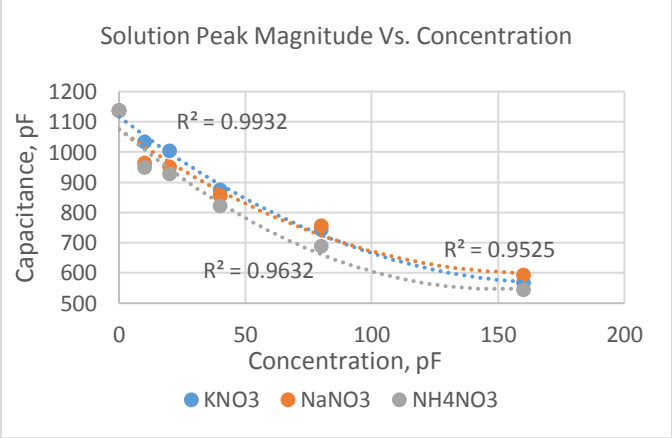

Fig. 10. A plot of solution peak magnitude versus concentration for each nitrate evaluated.

The relationships between resonant peak frequency and concentration were used to develop equations relating the frequency of the resonant peak to the concentration, for each nitrate type. For KNO_3, this equation is

$$C = 46.424f_p^2 - 4002.2f_p + 86247, \quad (1)$$

where C is nitrate concentration in ppm and f_p is the frequency of the sensor's resonant peak in MHz. For $NaNO_3$, the equation is

$$C = 91.469f_p^2 - 7774.4f_p + 165190, \quad (2)$$

and for NH_4NO_3, the equation is

$$C = 67.623f_p^2 - 5739.9f_p + 121796. \quad (3)$$

R^2 values provide a metric to evaluate the quality of the fit of an equation to the data. For (1) through (3), the associated R^2 values were 0.9977, 0.9875, and 0.9849, respectively. Similarly, the relationships between resonant peak magnitude and concentration were also used to develop equations relating the magnitude of the resonant peak to the concentration, for each nitrate type. For KNO_3, this equation is

$$C = 0.0004M_p^2 - 0.976M_p + 580.51, \quad (4)$$

where C is nitrate concentration in ppm and M_p is the magnitude of the sensor's resonant peak in pF. For $NaNO_3$, the equation is

$$C = 0.0006M_p^2 - 1.2841M_p + 722.49, \quad (5)$$

and for NH_4NO_3, the equation is

$$C = 0.0005M_p^2 - 1.1281M_p + 618.5. \quad (6)$$

For (4) through (6), the associated R^2 values were 0.9978, 0.9979, and 0.9959, respectively.

From the data in Table I, the plot in Fig. 11 was created of the magnitude of the resonant peak versus the frequency of the resonant peak for each nitrate and concentration evaluated with the PCB sensor. The plots reveal a linear relationship between magnitude and frequency of the resonant peaks as the concentrations varied, with R^2 values of 0.992 for KNO_3, 0.9751 for $NaNO_3$, and 0.954 for NH_4NO_3, respectively. The data in the plots in Figs 8, 9, and 10 illustrate that subtle differences exist between the responses of the PCB sensor in different types of nitrate solutions. However, all the nitrate solutions resulted in a discernable decrease in the resonant peak's magnitude and frequency as the concentration increased.

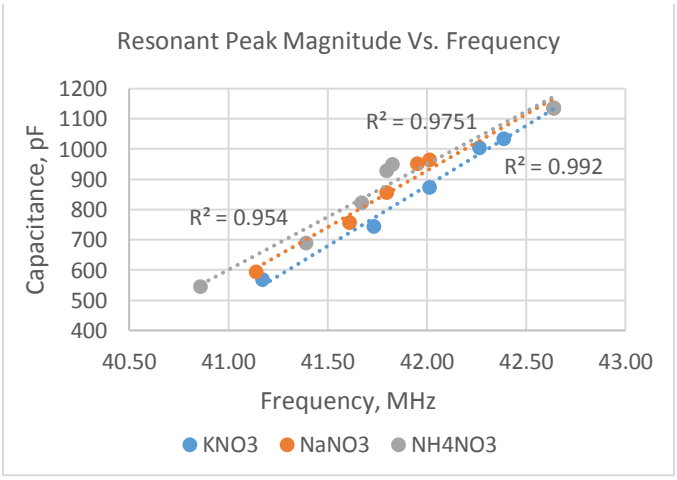

Fig. 11. A plot of resonant peak magnitude versus frequency.

V. Practical PCB Sensors

Low-cost PCB sensor technology has some characteristics and issues that need to be addressed to realize high-quality environmental sensors. The lowest cost PCBs are generally made using FR-4 E-glass substrates. FR-4 is made from layers of electrical grade fiberglass mesh that are bound together using an organic resin. As such, the FR-4 substrate absorbs moisture from its operating environment [18]. This characteristic would affect a sensor that is immersed in an aqueous solution for long periods of time. Circuit board coating materials can be used to minimize or even alleviate this issue. Additionally, PCB manufacturing tolerances need to be investigated for how small differences in trace widths, solder mask thicknesses, etc. affect sensor operation and if these differences can be accounted for through individual sensor calibration. This is illustrated in Fig. 12, where sensor parallel capacitance versus frequency curves are plotted for three identical PCB sensors tested in DI water. The curves are similar, with slightly different resonant peak magnitudes and frequencies. Also, since this type of sensor is affected by changes in temperature [19], measuring temperature and using it in adjusting the sensor data will improve the sensor's performance. Since the sensor is a circuit board, it is easy to integrate a discrete temperature sensor onto the PCB sensor.

Many techniques have been developed for instrumenting capacitive sensors. Since the capacitance values are relatively large compared to those of MEMS capacitive sensors, the interface circuitry can often be implemented using discrete components integrated directly onto the PCB sensor itself. Examples of relevant capacitive interface circuits include phase locked loops [20], sigma-delta capacitance-to-digital conversion [21], relative phase delay [22], and relaxation oscillators [23]. These improvements will be pursued in future versions of this nitrate sensor.

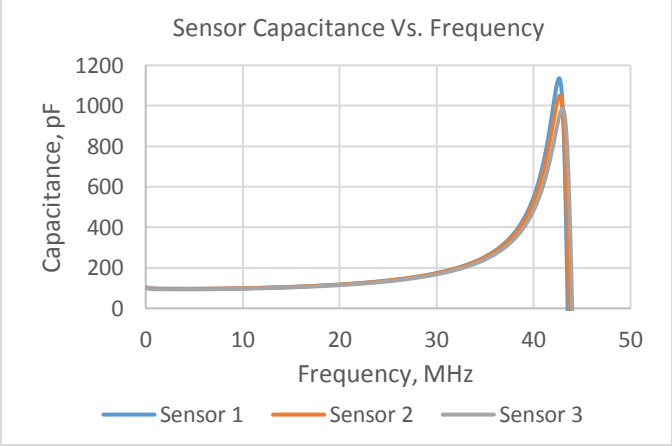

Fig. 12. A plot of sensor capacitance vs. frequency in DI water with three different PCB sensors.

VI. Conclusion

Low-cost nitrate sensors would be useful for improving pollution detection and optimizing the use of nitrate based fertilizers. PCB sensor technology is being used to realize a variety of low-cost environmental sensors. Employing electrochemical impedance spectroscopy, a frequency swept interdigitated PCB sensor, manufactured in a commercial low-cost PCB process, was demonstrated to detect nitrates in DI water at concentrations between 0 and 160 ppm, for potassium nitrate, sodium nitrate, and ammonium nitrate, respectively. The sensor produced a capacitance versus frequency signature with a characteristic resonant peak that decreased in magnitude and frequency as the nitrate concentration increased. From this data, models were produced that predict nitrate concentration from resonant peak magnitude and frequency. When compared to the experimentally collected data, all of the derived models had R^2 values greater than 0.95.

References

[1] M.D. Cruz, J. Glick, S.H. Merker, and D. Vearrier, "Survival after severe methemoglobinemia secondary to sodium nitrate ingestion," Toxicology Communications, vol. 2, no. 1, pp. 21-23, 2018.

[2] R.R. Gu, M.K. Sahu, and M.K. Jha, "Simulating the impacts of bio-fuel crop production on nonpoint source polltion in the upper Mississippi river basin," Ecological Engineering, vol. 74, pp. 223-229, 2015.

[3] P.K. Sahoo, K. Kim, and M.A. Powell, "Managing groundwater nitrate contamination from livestock farms: implication for nitrate management guidelines," Curr. Pollution Rep., vol. 2, pp. 178-187, 2016.

[4] S.E. Hobbie, J.C. Finlay, B.D. Janke, D.A. Nidzgorski, D.B. Millet, and L. A. Baker, "Contrasting nitrogen and phosphorus budgets in urban watersheds and implications for managing urban water pollution," PNAS, vol. 114, no. 20, pp. 4177-4182, 2017.

[5] C.S. Jones, J.K. Nielsen, K.E. Schilling, and L.J. Weber, "Iowa stream nitrate and the Gulf of Mexico," PLoS One, vol. 13, No. 4, 8pp, 2018.

[6] N.F. Nazarudin, M.A.M. Noor, N.A. Rashid, G. Witjaksono, and N.A. Nayan, "Characterization of acrylate-based chemFET sensor for nitrate sensing and monitoring," Proc. of the 2014 IEEE Conf. on Biomedical Engineering and Sciences, Minri, Malaysia, Dec. 8-10, 2014, pp. 154-158.

[7] V.A.T. Dam and M.A.G. Zevenbergen, "Low cost nitrate sensor for agricultural applications," Proc. of TRANSDUCERS & EUROSENSORS XXXIII, Berlin, Germany, Jun. 23-27, 2019, pp. 1286-1288.

[8] G. Dong, W. Zhang, R. Yang, Y. Yang, Y. Yu, and X. Zhang, "Determination of nitrate nitrogen in soil based on K ratio spectrophotometry," Proc. of the 2014 4th Int. Conf. on Instrumentation, Computer, Communication and Control, Harbin, China, Sept. 18-20, 2014, pp. 544-547.

[9] N.M. Razili, S. Ambran, A. Hamzah, N. Abdullah, O. Mikami, H. Hara, M.Q. Lokman and M.H. Yaacob, "Etched fiber Bragg grating sensor for nitrate sensing application," Proc. of the 2018 IEEE 7th Int. Conf. on Photonics, Kuah, Malaysia, April 9-11, 2018, 3pp.

[10] M.E.E. Alahi, L. Xie, S. Mukhopadhyay, and L. Burkitt, "A temperature-compensated smart nitrate-sensor for agricultural industry," IEEE Tran. on Industrial Electronics, vol. 64, no. 9, pp. 7333-7341, Sept. 2017.

[11] HORIBA LAQUAtwin NO3-11 Compact Nitrate Ion Meter, https://www.horiba.com/us/en/scientific/horiba-instruments/.

[12] Hanna Instruments HI7609829-12 Nitrate Ion Selective Electrode, www.hannainst.com.

[13] R.N. Dean and F.T. Werner, "A PCB environmental sensor for use in monitoring drought conditions in estuaries," J. of Microelectronics and Electronic Packaging, vol. 13, pp. 182-187. 2016.

[14] E.F. da Costa, N.E. de Oliveira, F.J.O. Morais, P. Carvalhaes-Dias, L.F.C. Duarte, A. Cabot, and J.A.S. Dias, "A self-powered and autonomous fringing field capacitive sensor integrated into a micro sprinkler spinner to measure soil water content," MDPI Sensors, vol. 17, pp. 575-520, 2017.

[15] X. Wang, Y. Wang, H. Leung. S. Mukhopadyay, M. Tian, and J. Zhou, "Inorganic material detection based on electrode sensor," IEEE Sensors J., vol. 16, no. 11, pp. 4147-4148, 2016.

[16] G. Chighladze, A. Kaleita and S. Birrell, "Sensitivity of capacitance soil moisture sensors to nitrate ions in soil solution," J. of Soil Physics, vol. 74, no. 6, pp. 1987-1995, 2010.

[17] R.N. Dean, "A frequency swept low-cost capacitive fringing field PCB sensor," Proc. of the IMAPS 50th International Symposium on Microelectronics, Raleigh, NC, Oct. 9-12, 2017, pp. 157-162.

[18] M.G. Pecht, H. Ardebili, A.A. Shukla, J.K. Hagge and D. Jennings, "Moisture ingress into organic laminates," IEEE Trans. on Components and Packaging Technology, vol. 22, no. 1, pp. 104-110, March 1999.

[19] R.N. Dean, A.K. Rane, M.E. Baginski, J. Richard, Z. Hartzog, and D.J. Elton, "A capacitive fringing field sensor design for moisture measurement based on printed circuit board technology," IEEE Tran. on Instrumentation and Measurement, vol. 61, no. 4, pp 1105-1111, April 2012.

[20] S. Nonta, A. Keawphusuk, and P. Wardkein, "Measuring on sugar content of sugarcane based on phase locked loop with capacitive sensor," J. Phys.: Conf. Ser., vol. 1039, 5pp, 2018.

[21] D. Garcia-Lesta, E. Ferro, V.M. Brea, P. Lopez, D. Cabello, J. Iglesias, and J. Castillejo, "Capacitance-based wireless sensor mote for snail pest detection," Proc. 2015 IEEE Sensors Applications Conference, Zadar, Croatia, Apr. 13-15, 2015, 6pp.

[22] Y. Meng and R.N. Dean, "A technique for improving the linear operating range for a relative phase delay capacitive sensor interface circuit," IEEE Trans. on Instrumentation and Measurement, Vol. 65, No. 3, March 2016, pp. 624-630.

[23] R.N. McIntosh and M.E. Casada, "Fringing field capacitance sensor for measuring moisture content of agricultural commodities," IEEE Sensors J., vol. 8, no. 3, pp. 240-247, March 2008.